EarthArXiv Coversheet

Claire Masteller[1]

[1]*Earth, Environmental, and Planetary Sciences, Washington University in St. Louis, St. Louis, MO, USA*

cmasteller@wustl.edu

This pre-print is in review at *Journal of Geophysical Research – Earth Surface* and has undergone one round of peer-review.

Downstream patterns in bedrock valley morphology encode climatic and tectonic forcing

Claire C. Masteller[1]

[1]Department of Earth, Environmental, and Planetary Sciences, Washington University in St. Louis.

Corresponding author: Claire C. Masteller (cmasteller@wustl.edu)

Key Points:

- Catchment-scale patterns in bedrock valley confinement capture the relative influence of vertical and lateral erosion processes.
- We develop a new profile model for downstream patterns in bedrock valley morphology with varying uplift, climate, and erodibility.
- Modeled profiles agree with observed differences in valley morphology for basins spanning an uplift and orographic precipitation gradient.

Abstract

Fluvially-carved bedrock valleys are ubiquitous landscape features. Vertical incision into underlying bedrock generates valley relief, whereas lateral migration of the river channel widens the valley floor as the river erodes the valley walls. The relative efficacy of these processes, which can be modulated by precipitation and water discharge, sediment supply, lithology, and uplift rates is recorded by the relationship between valley width, channel width, and valley relief at a cross-section. Numerous studies have interpreted differences in bedrock valley morphology to be evidence for variability in tectonics, climate, or geology, or as evidence of landscape disequilibrium. However, expected downstream covariation of these parameters under steady-state conditions has not been yet thoroughly explored. This contribution develops a 1-D profile model to describe expected downstream coevolution of channel width, valley width, and valley relief, described holistically using a valley confinement index. Model predictions agree well with data from seven catchments in the King Range, CA spanning a gradient in tectonic uplift and precipitation. Systematic variations in valley morphology correspond with differences in the Erosion number between catchments, which summarizes the combined effect of multiple factors that influence fluvial bedrock incision. These results suggest that longitudinal patterns in bedrock valley morphology provide a promising, holistic metric to interpret the relative influence of tectonics, climate, and lithology on bedrock valley formation in detachment-limited landscapes.

Plain Language Summary

Rivers continuously sculpt the bedrock valleys in which they reside via erosion. Valleys are created through two main processes: vertical erosion into bedrock, which forms the valley relief,

and lateral migration of the river across the valley floor, widening the valley as it erodes the valley walls. The relative influence of these processes results in a wide range of valley forms, from narrow, plunging canyons to expansive valleys that are many times wider than the channels that have carved them. Past research has linked differences in valley shapes to tectonics, climate, or geology. However, to our knowledge, there is no expectation for how valley shape, specifically the relationship between river channel width, valley width, and valley relief, changes downstream within a river basin. We develop a simple model to describe downstream changes in valley shape under a range of scenarios capturing differences in uplift, precipitation, and rock strength. We find that model results align well with actual data from river basins with varying tectonic uplift and precipitation. We propose that analysis of downstream patterns in valley shape offers a comprehensive lens through which the combined influence of tectonics, climate, and geology affects river erosion and the evolution of bedrock landscapes.

1 Introduction

Fluvially-carved bedrock valleys are ubiquitous landscape features across Earth's surface (Montgomery, 2002). Valleys form and evolve through a combination of lateral and vertical fluvial erosion processes. Vertical incision of the channel into the underlying bedrock generates catchment or valley relief (Brocard & van der Beek, 2006; Stock et al., 2005; Willett, 2010), whereas lateral migration of the river widens a valley as the river interacts with and erodes the valley walls (e.g. Bufe et al., 2016, 2017; Langston & Tucker, 2018; Malatesta et al., 2017). The relative efficacy of these processes, which can be modulated by precipitation and water discharge, sediment supply, lithology, and tectonic uplift, is thus embedded in bedrock valley morphology - specifically in the relationship between valley width, channel width, and valley relief (e.g. Limaye and Lamb, 2014). Because these aspects of valley morphology are linked

through fluvial processes, they are not independent descriptions of landscape form. Rather, channel width, valley width, and valley relief coevolve, reflecting the long-term partitioning of vertical incision and lateral channel migration and underlying geomorphic process links.

The longitudinal elevation profile of the main stem river channel within a watershed is commonly used to infer variability in tectonic uplift, rock erodibility, and climatic forcing between watersheds, as well as to identify landscape disequilibrium within individual catchments (Frankel et al., 2007; Kirby & Whipple, 2012; Snyder, 2000; Wobus et al., 2006). While the river channel elevation profile is most often used, previous studies have also explored the control of climate and tectonics on channel width, valley width, and valley relief. Rivers in more rapidly uplifting landscapes tend to be relatively narrow for a given water discharge, this narrowing helps to increase the boundary shear stress active on the channel bed, allowing erosion to keep pace with uplift (e.g. Finnegan et al., 2005). More recently, variations in valley width between valley cross-sections has also been shown to reflect differences in climatic forcing (Hancock & Anderson, 2002; He et al., 2026; Mackin, 1937; Van Appledorn et al., 2019; Wegmann & Pazzaglia, 2002), uplift (Bufe et al., 2016; Clubb et al., 2023), sediment supply (Brocard & van der Beek, 2006; Finnegan & Balco, 2013; Langston & Robertson, 2023; Schanz et al., 2019; Tofelde et al., 2022), and rock strength (Brocard & van der Beek, 2006; Bursztyn et al., 2015; Keen-Zebert et al., 2017; Langston & Temme, 2019; Ortega-Becerril et al., 2018; Schanz & Montgomery, 2016; Wohl, 2008; Zondervan et al., 2024). Recent work has further emphasized that downstream changes in valley with reflect the cumulative balance between lateral erosion and vertical incision (Clubb et al., 2022; Snyder et al., 2003; Tomkin et al., 2003; Turowski et al., 2024). In this view, the rate of downstream valley widening has been interpreted has been interpreted to reflect catchment-scale differences in tectonic uplift rates, sediment supply, and

rock strength (Beeson et al., 2018; Clubb et al., 2023; May et al., 2013; Schanz & Montgomery, 2016). While these interpretations are largely empirical, a recent physics-based model for valley widening hypothesized that the rate of downstream widening may be controlled by the ratio of lateral sediment transport capacity relative to uplift (Turowski et al., 2024). Deviations from these expected downstream patterns in valley width have also been used as evidence for ongoing drainage basin reorganization and landscape disequilibrium (e.g. Harel et al., 2022). Valley relief also generally increases in areas with increased uplift due to enhanced bedrock river incision (Finnegan et al., 2008; Montgomery & Brandon, 2002). While each of these geomorphic features has been cited individually as an expression of climate or tectonics at the landscape scale - the covariation of channel width, valley width, and valley relief, and spatial structure of this covariation remains less thoroughly explored.

Limaye and Lamb (2014) demonstrated that a process-based fluvial erosion model incorporating both lateral and vertical erosion processes could produce a range of relationships between bedrock valley width, channel width, and valley relief at individual cross-sections. In their model, valley morphology emerges from the coevolution of channel lateral migration and vertical incision, mediated by variations in bank erodibility driven by sediment cover, together control the resulting valley form. This process-based perspective highlights that valley morphology is not defined by any single metric but instead reflects the coupled adjustment of channel and valley geometry through time. Limaye and Lamb (2014) quantified resultant differences in bedrock valley morphology using a dimensionless bedrock valley confinement index, w_v^*, defined as

$$w_v^* = \frac{w_v - w_c}{r}, \quad (1)$$

where the numerator, $w_v - w_c$ is relative valley width, where w_v is valley width, w_c is channel width, and r is valley relief. Larger values of w_v^* are associated with low confinement, or wide valleys with low relief and smaller values of w_v^* are associated with narrow valleys with high relief, or highly confined valleys (Fig. 1A). Previous studies have used a similar metric, valley aspect ratio, w_v/r, to quantify valley shape (e.g. Langston & Temme, 2019). However, valley confinement index, w_v^* explicitly captures the fraction of the valley floor occupied by the active channel. This is particularly informative in situations where relative valley width ($w_v - w_c$), varies across a catchment or in scenarios where channel width and valley width do not change in proportion with one another downstream (Fig. 1B).

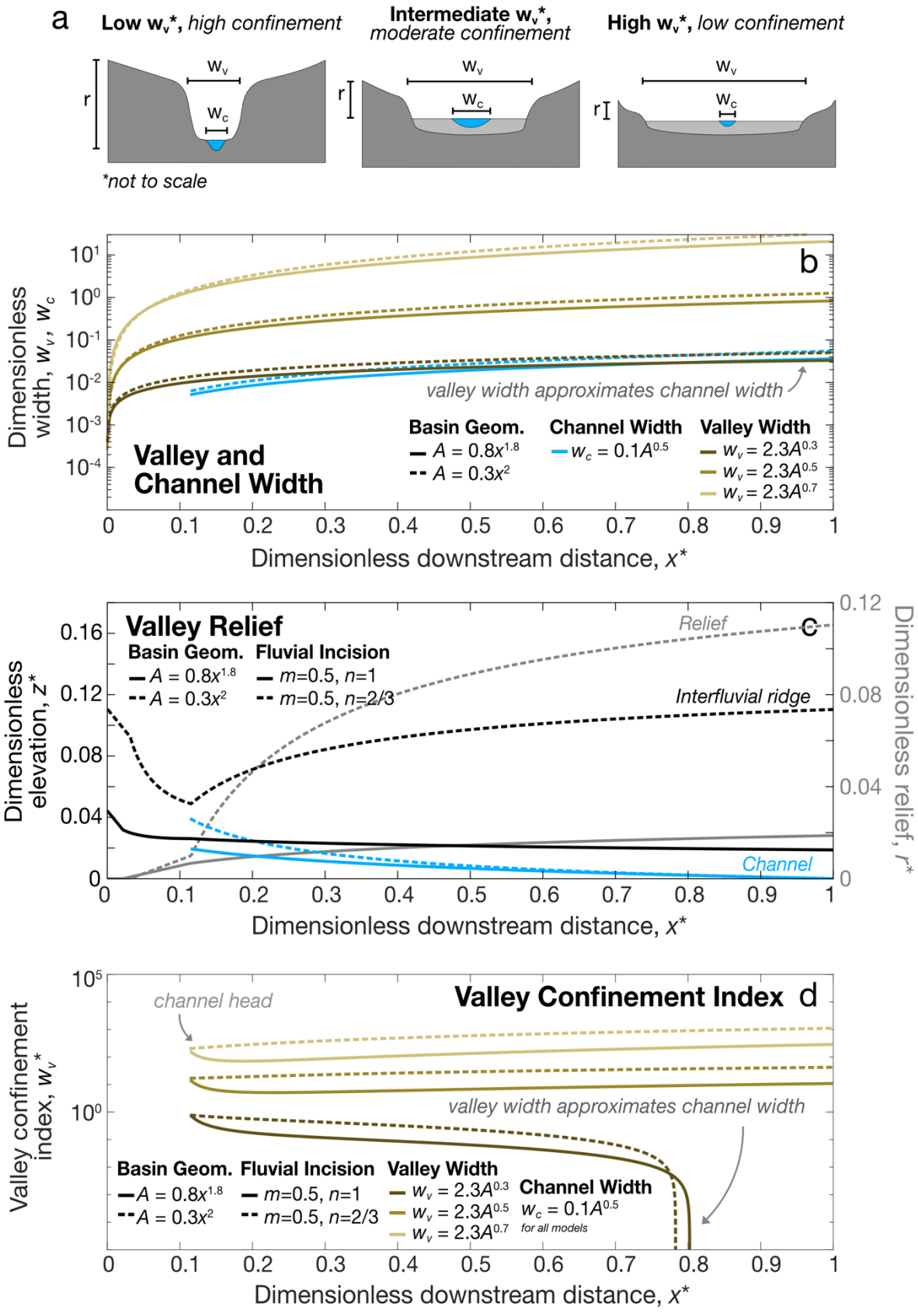
a
Low w_v*, high confinement
Intermediate w_v*, moderate confinement
High w_v*, low confinement
w_v
w_c
r
*not to scale
b
Valley and Channel Width
Dimensionless width, w_v, w_c
valley width approximates channel width
Basin Geom.
$A = 0.8x^{1.8}$
$A = 0.3x^2$
Channel Width
$w_c = 0.1A^{0.5}$
Valley Width
$w_v = 2.3A^{0.3}$
$w_v = 2.3A^{0.5}$
$w_v = 2.3A^{0.7}$
Dimensionless downstream distance, x^*
Valley Relief
c
Relief
Interfluvial ridge
Channel
Basin Geom.
Fluvial Incision
m=0.5, n=1
m=0.5, n=2/3
Dimensionless elevation, z^*
Dimensionless relief, r^*
Valley Confinement Index
d
channel head
valley width approximates channel width
Valley confinement index, w_v^*
for all models

Figure 1. Valley confinement index, w_v^* , and its components. A) Schematic illustration of bedrock valley morphology for valleys with low, intermediate, and high w_v^*; B) Dimensionless channel width, w_c, (blue) and valley width, w_v (tan shades), w_c and w_v are normalized by their respective maximum values at $x*$ for schematic purposes only. A range of downstream valley-widening rates for two distinct Hack's Law scaling relationships (solid and dashed lines); C) Channel (blue) and interfluvial ridge (black) elevation profiles and associated downstream relief profiles (gray) for two distinct combinations of Hack's Law and the stream power incision model (solid and dashed lines) and an erosion number, N_e=0.3. Similar to B) relief has been normalized by $x*$ for schematic purposes only. D) Valley confinement index, w_v^*, profiles derived from profiles in B and C.

Robust attribution of the relative influence of lateral and vertical erosion processes, and their associated drivers, on catchment-scale differences in bedrock valley morphology requires an underpinning steady state expectation, or null hypothesis, for each combination of driving variables. This contribution develops a relatively simple expectation for downstream patterns in bedrock valley confinement index by combining empirical channel width- and valley width-drainage area scaling relationships with a 1-D profile model for interfluvial ridge height from Willett (2010) derived from the stream power incision model (SPIM) (See Equation 10 in Willett, 2010). Modeled profiles of valley confinement index with downstream distance are compared to data from seven catchments in the King Range, CA spanning a gradient in tectonic uplift and precipitation (Merritts & Bull, 1989; Snyder et al., 2003). This comparison demonstrates that first-order differences in bedrock valley morphology, characterized by downstream profiles of w_v^*, can predictably record differences in climatic and tectonic forcing.

These results provide a new 1-D modeling framework that can be applied to more definitively attribute catchment-scale patterns in bedrock valley morphology to specific drivers such as tectonics, climate, and erodibility, and for identifying disequilibrium conditions and ongoing landscape adjustment within a river valley.

2 Methods

2.1 Model Framework for Downstream Valley Confinement Profiles

The 1D profile model for steady state bedrock valley confinement index, w_v^*, is developed by combining empirical scaling relationships for channel width, w_c, (Leopold & Maddock, 1953) and valley width, w_v, (Beeson et al., 2018; Clubb et al., 2022; Langston & Tucker, 2018) with expected profiles in valley relief, r, (Willett, 2010) derived from the stream power incision model (SPIM). As such, this formulation represents the baseline detachment-limited assumption, providing a reference case that assumes limited effects of sediment cover on catchment-scale patterns in valley morphology.

Channel width, w_c, robustly scales with increasing downstream discharge, Q, (e.g. Ferguson, 1986; Gleason, 2015; Leopold & Maddock, 1953; Métivier et al., 2017; Phillips et al., 2022), or with drainage area, A, assuming Q scales linearly with increasing A (e.g. Dunne and Leopold, 1978; Whipple, 2004). Substantial empirical work demonstrates that downstream width-discharge scaling is well-defined by a power-law with the form $w_c = k_c Q^b$, or

$$w_c = k_c A^b, \quad (2)$$

where b~0.4-0.5 for alluvial rivers (Fig 1B; Anderson et al., 2004; Leopold & Maddock, 1953; Moody & Troutman, 2002; Whitbread et al., 2015), though more recent studies show a wider range of scaling relationships across individual watersheds (Allmendinger et al., 2005; Anderson et al., 2004; Kostynick et al., 2026; Masteller et al., n.d.; Phillips et al., 2024). Similar

channel width-drainage area (w_c- A) scaling exponents have been measured for bedrock rivers, where b~0.3-0.5 (Whipple, 2004; Wohl & David, 2008) and may vary with rock resistance (Montgomery & Gran, 2001; Wohl, 2004) and uplift rate, though the latter has not been shown consistently (Pazzaglia & Brandon, 2001; Tomkin et al., 2003).

Because bedrock valleys are formed by the rivers that incise them, it is not surprising that downstream changes in valley width can similarly be expressed as a function of discharge, or more commonly, drainage area, as $w_v = k_v Q^c$, or

$$w_v = k_v A^c, \quad (3)$$

where, in most cases, c~0.2 to 0.6, bracketing the observed values for channel width-drainage area scaling exponents (Fig 1B; Beeson et al., 2018; Clubb et al., 2022; Langston & Temme, 2019; Snyder et al., 2003; Tomkin et al., 2003; see Turowski et al., 2024 for a summary). The valley width-drainage area (w_v- A) scaling exponent c has been shown to vary with rock resistance (e.g. Langston and Temme, 2019), sediment supply (e.g. Beeson et al., 2018), or uplift rate (e.g. Clubb et al., 2023). Landscape evolution models that incorporate lateral erosion have produced a similar range of downstream valley widening exponents to these empirical studies, with c ranging from 0.3 to 0.7 (Langston and Tucker, 2018).

While there is general overlap between channel and valley width-drainage area (w_c-A and w_v-A, respectively) scaling relationships, differences between downstream widening rates, primarily captured by differences in the scaling exponents, c and b, can result in continuously increasing or decreasing relative valley width (w_v- w_c) within a bedrock valley. Relative valley width will increase downstream if valley-widening outpaces channel-widening ($c>b$). Whereas, if downstream channel-widening outpaces valley-widening ($c<b$), relative valley width will decrease downstream as the river channel continues to occupy a larger and larger fraction of the

valley floor. To our knowledge, how downstream valley and channel widening covary – as reflected in their respective width-drainage area scaling relationships – and what controls these relative rates remain largely unexplored.

Generation of bedrock valley relief is driven by ongoing fluvial incision in actively uplifting orogens. In detachment-limited cases, the steady-state channel longitudinal profile is well-described using the stream-power incision model (SPIM), where bedrock incision can be calculated as

$$E = KA^m S^n, \quad (4)$$

where K is rock erodibility, which can include climatic effects (e.g. Ferrier et al., 2013), A is catchment drainage area, S is local slope, and m and n are empirical scaling exponents (Howard, 1994; Whipple, 2004; Whipple & Tucker, 1999). Embedded within this formulation is the implicit assumption that channel width follows the downstream hydraulic geometry relationship described by Equation 2, such that width increases systematically with drainage area, typically with $b \approx 0.5$. Under steady state conditions, bedrock incision, E, can be directly related to tectonic uplift rate, U, such that bedrock incision rates increase with more rapid uplift (Duvall, 2004; Kirby & Whipple, 2012; Wobus et al., 2006). Willet (2010) modeled interfluvial ridge height for this steady state case using a combination of SPIM and Hack's Law, which accounts for the structure of the river channel network within a catchment with the form

$$A = k_r x^h, \quad (5)$$

where x is downstream channel length from the divide, and k_r and h are empirical constants (Hack, 1957; Montgomery & Dietrich, 1992; Rigon et al., 1996). Due to the nonlinear nature of both SPIM and Hack's Law, modeled interfluvial ridge profiles can take a variety of forms, from concave ridge profiles mirroring the channel itself to convex ridge profiles with

enhanced increases in catchment relief downstream (Fig. 1C; See Equation 10 in Willet, 2010). To account for the controls of tectonic uplift (U), precipitation (P), and rock strength (K), Willet (2010) employs a dimensionless "Erosion number", N_e, where

$$N_e = \left(\frac{U}{x_d^{hm} K P^m k_r^m}\right)^{1/n} \quad (6)$$

and x_d is the total length of the river (Willett, 1999). N_e ultimately acts as a scaling factor for interfluvial ridge height, where higher N_e values increase interfluvial ridge heights relative to the channel elevation profile, enhancing relief (calculated as the elevation difference between the channel and the ridgeline) throughout a catchment. An advantage of N_e in a modeling context is that it summarizes the combined effect of multiple factors that influence fluvial bedrock incision rates, allowing for a general prediction of interfluvial ridge height, while also allows for individual drivers to be treated separately.

Downstream profiles of bedrock valley confinement index, w_v^* (Eq. 1), are calculated from channel width, valley width, and valley relief, where each is individually calculated as a function of drainage area, A. Bedrock valley confinement index is reprojected to downstream distance using Hack's Law and nondimensionalized by total stream length to yield profiles in dimensionless distance, x^* (Fig. 1D). Because w_v^* combines multiple nonlinear relationships, downstream patterns are expected to be similarly nonlinear. Although potentially more complex than individual morphologic metrics, these elements are likely covary, as relief generation, valley widening, and channel widening are all governed by fluvial erosion processes (Limaye and Lamb, 2014). As such, downstream patterns in w_v^* provide a useful framework for evaluating the relative efficacy of lateral and vertical erosion towards a more holistic description of downstream evolution of valley morphology.

To explore the range of downstream patterns in bedrock valley confinement that may arise in steady state, detachment-limited landscapes, this contribution generates w_v^* profiles for a combination of valley width-drainage area scaling exponents, Hack's Law relationships, SPIM exponents m and n, and Erosion number values. To reduce the number of free parameters in this initial exploration, the model assumes a common drainage area scaling for channel width, $w_c = 0.1A^{0.5}$. Valley width is calculated as $w_v = 2.3A^c$ (Langston & Tucker, 2018). Although the coefficients used in these relationships can vary widely (e.g. Turowksi et al., 2024), constant values are adopted here to isolate first-order downstream trends. This contribution first considers two end-member scenarios, (1) valley widening outpaces channel widening (c=0.7, b=0.5) and (2) channel widening outpaces valley widening, (c=0.3, b=0.5) (Fig. 2). It is worth noting here that even valley and channel widening exponents are equal (c=0.5, b=0.5), the larger coefficient in the valley-width relationship still produces downstream increases in relative valley width, yielding patterns comparable to the second end-member case (Fig. 1B, Supplementary Information). Catchment relief profiles are then calculated using two combinations of Hack's Law and SPIM exponents following Willet (2010): producing one concave ridge profile ($A = 0.8x^{1.8}$, m=0.5, and n=1) and one convex ridge profile ($A = 0.3x^2$, m=0.5, and n=2/3) (Fig. 1C). Finally, these components are combined to calculate w_v^* profiles across Erosion numbers spanning five orders of magnitude, N_e=10^{-5} to 3.

2.2 Constraining bedrock valley confinement for catchments in the King Range, CA

To assess the performance of both the w_v^* metric and the modeling framework developed here, modeled w_v^* profiles to downstream patterns in bedrock valley confinement for seven catchments in the King Range in northern California (Fig. 2). Profiles in w_v^* for the King Range

254 catchments are derived using field-derived valley and channel width-drainage area scaling-
255 relationships (Snyder, 2000; Snyder et al., 2003; Supplementary Information) and bedrock valley
256 relief profiles extracted from Digital Elevation Model (DEM) topography. These catchments are
257 selected because prior work suggests that channel slopes are close to steady state and are well
258 described by detachment-limited incision when erosion thresholds and discharge variability are
259 taken into account (Snyder et al., 2000; 2003). Further, there is a wealth of existing precipitation,
260 uplift, geologic, and geomorphic data available for the region (e.g. Merritts & Bull, 1989;
261 Snyder, 2000; Snyder et al., 2003; Whipple, 2004).

262 Downstream w_v^* profiles are calculated using previously published valley and channel
263 width-drainage area scaling relationships from Snyder et al., (2000). Contributing drainage area
264 is extracted along the main stem channel of each river from 1-m resolution USGS 3DEP DEMs
265 (US Geological Survey) using Topotoolbox, a Matlab-based topographic analysis package
266 (Schwanghart & Scherler, 2014). Expected downstream valley and channel widths are then
267 computed from the reported drainage area scaling relationships. Catchment relief is calculated by
268 extracting catchment ridgelines and projecting ridge elevations onto the trunk channel using the
269 shortest Euclidean distance between the ridge and channel network. Relief at each point along
270 the long profile is defined as the difference between local maximum ridge elevation and trunk
271 channel elevation. To facilitate comparison across catchments, all profiles are normalized by
272 total mainstem length. Resulting downstream profiles in valley width, channel width, and relief
273 are then combined to calculate w_v^* as a function of dimensionless downstream distance, x^*.

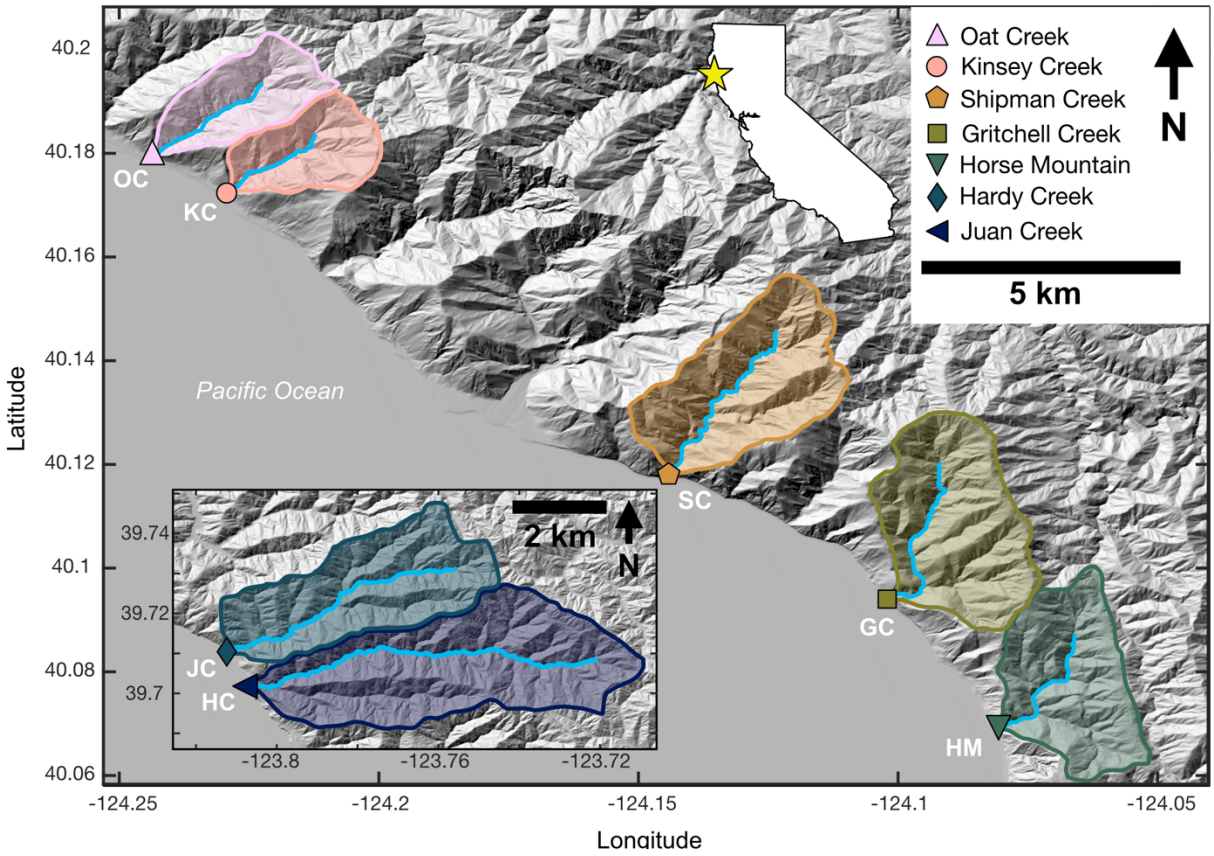

Figure 2. Map of King Range catchments used in this study with southern catchments, Juan Creek and Hardy Creek, displayed in the inset. Colors reflect a gradient in calculated Erosion number, where pinks indicate high N_e and blues indicate low N_e.

The extensive prior work in the King Range, allows for the calculation of catchment-specific Erosion numbers using Equation 6 (Merritts & Bull, 1989; Merritts, 1996; Snyder et al., 2003, summarized in Supplementary Information). The study catchments span a tectonic uplift gradient from ~0.5 mm/year in the southern catchments to ~4 mm/year in the northern catchments. Orographic precipitation similarly increases northward, with mean annual precipitation ranging from ~1.5 to 3 m/yr. All catchments are underlain by similarly erodible Franciscan mélange lithology. Catchment-specific erodibility values reported by Snyder et al. (2003), which range from K =3.7×10^{-5} to 9.6×10^{-4} m$^{0.14}$/yr, assuming $m = 0.43$ and $n = 1$.

286 Catchment-specific Hack's Law parameters are derived using TopoToolbox and used to
287 calculate N_e(see Supplementary Information). Calculated Erosion numbers decrease
288 systematically from north to south, ranging from N_e=5.07×10^{-2} for Oat Creek to a minimum
289 N_e=1.02×10^{-4} for Hardy Creek (Table 1). Although precipitation and erodibility vary across the
290 region, spatial variability in N_e primarily reflects the strong north-south gradient in tectonic
291 uplift.

292 **Table 1**. Calculated Erosion Numbers, N_e, for King Range study catchments

Catchment Name (North to South)	**Erosion Number, N_e**
Oat Creek	5.07×10^{-2}
Kinsey Creek	5.00×10^{-2}
Shipman Creek	1.95×10^{-2}
Gritchell Creek	1.52×10^{-2}
Horse Mountain	6.31×10^{-3}
Hardy Creek	1.29×10^{-4}
Juan Creek	2.89×10^{-4}

293

294 *2.3 Metrics for model-data comparison of bedrock valley confinement*

295 For comparison with the King Range catchments, the downstream channel-width scaling
296 exponent in the profile model is modified from $b = 0.5$ to $b = 0.35$ to better reflect the average
297 value reported by Snyder et al. (2003). We then apply a range of valley width-drainage area
298 scaling exponents, c =0.2-0.5, again consistent with the range reported originally by Snyder et
299 al., (2003). Hack's Law relationships and SPIM parameters are retained from the initial end-
300 member models. Erosion numbers are varied from N_e=10^{-6} to 10.

301 It is worth acknowledging that while the model could be calibrated individually for each
302 catchment, the aim of this contribution is to evaluate the general behavior and utility of the
303 simplified w_v^*framework rather than reproduce observations exactly. Catchment-specific

304 calibration would require simultaneous adjustment of numerous empirical scaling coefficients
305 and exponents, obscuring the relative influence of downstream valley widening, channel
306 widening, and relief generation on valley form. Because general parameter values are used for
307 aspects of the modeling (e.g. valley and channel width-drainage area scaling coefficients)
308 modeled w_v^* values are not expected to match observations directly. Rather, comparison presented
309 here focuses on whether downstream trends in bedrock valley confinement and the relationship
310 to N_e is reproduced consistently across both profile models and King Range data.

311 Comparison between modeled and field-derived w_v^* profiles focuses on two distinct
312 metrics: 1) a normalized median w_v^* and 2) a normalized residual confinement index ($NRCI$). For
313 both the King Range data and the suite of modeled profiles, w_v^* is normalized by the maximum
314 value in each dataset to facilitate comparison. Because N_e directly scales relief generation,
315 increasing N_e decreases median w_v^* and produces more confined valleys. For a given N_e, median
316 w_v^* is also influenced by differences between valley- and channel-widening rates, whether driven
317 by scaling exponents or coefficients. In both cases, larger disparities between valley and channel
318 widening increase median w_v^*, indicating reduced valley confinement. Importantly, the simplified
319 framework developed here treats relief generation, valley widening, and channel widening
320 independently, likely producing a broader range of confinement states than would occur if these
321 processes were tightly coupled. This approach intentionally explores the broadest possible
322 parameter space describing downstream patterns in valley confinement. As such, comparison of
323 these results with more mechanistic approaches (e.g. Limaye and Lamb, 2014; Turowski et al.,
324 2024) may help to provide further insight regarding the relative strength of the coupling between
325 these processes under differing climatic, tectonic, or geologic forcing.

The normalized residual confinement index (*NRCI*) metric is introduced to characterize overall differences in the shape of w_v^* profiles. This metric is adapted from the normalized concavity index (*NCI*), developed for river longitudinal profiles (described in Chen et al., 2019). Following this approach, a straight line to each log-transformed w_v^* profile from x^*=0.1 and 0.9 to minimize edge effects related to channel initiation in the headwaters or as the channels exit the King Range and reach the coastline. The integrated difference between the log-transformed w_v^* profile and straight line fit is then calculated, representing the residual valley confinement for the whole of the w_v^* profile (Fig. 5B insets, Supplementary Information). Values are then normalized by the maximum value within the modeled and field-derived datasets prior to comparison to produce a final *NRCI* metric. Negative *NRCI* values indicate concave-up w_v^* profiles, whereas positive *NRCI* values indicate convex profiles. High relief catchments associated with efficient fluvial incision and high N_e, are expected to exhibit concave w_v^* profiles (e.g. Fig. 1D) and negative *NRCI* values. In contrast, low relief catchments with wide valleys, associated with more efficient lateral erosion and low N_e, should exhibit convex w_v^* profiles (e.g. Fig. 1D) and positive *NRCI* values.

3 Results

3.1 *Modeled downstream trends in bedrock valley confinement*

Modeled w_v^* profiles are primarily controlled by the balance between valley widening and channel widening, captured by the relative magnitudes of the w_v-A and w_c-A scaling exponents (c and b), and by the Erosion number, N_e (Fig. 3). While variations in Hack's Law and SPIM parameters produce slight differences in w_v^* values and profile shapes, these effects are secondary (Fig. 3). Both end-member cases, show an initial downstream decrease in w_v^*,

reflecting increasing valley confinement near channel heads when N_e exceeds ~10^{-3}. This upstream behavior arises because fluvial incision rapidly generates relief as channels initiate while drainage area, and by extension, channel width and valley width, remain low. As a result, upstream patterns in w_v^* are predominately set by the shape of the ridge profile (e.g. Fig. 1C).

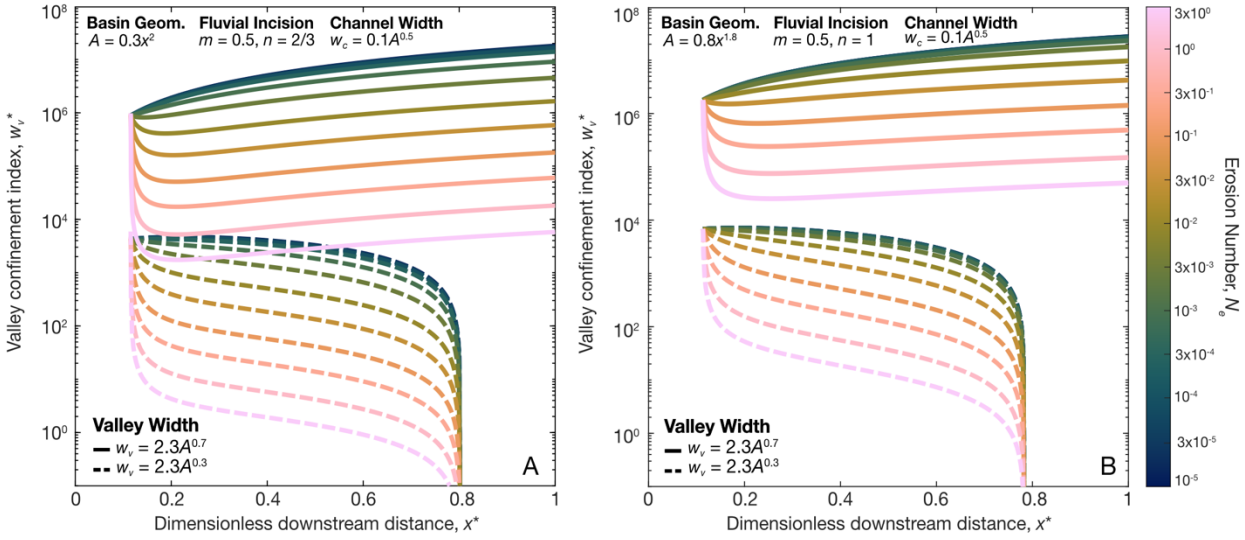

Figure 3. A) Downstream profiles of valley confinement index, w_v* for a case where downstream valley widening outpaces downstream channel widening (solid line) and where downstream channel widening outpaced valley widening (dashed line) for a range of N_e values (line color). B) Same as A, but with Hack's Law scaling, A = 0.8L$^{1.8}$, and stream power incision parameters, *m=0.5* and *n=1*. Colors denoting modeled Erosion Numbers, N_e, use the *batlow* color ramp (Crameri, 2023).

For the first end member case, where downstream channel widening outpaces valley widening (c=0.3, b=0.5) generally decreases downstream as the river progressively occupies a larger and larger fraction of the valley floor. This behavior is consistent with landscapes where

relatively efficient vertical incision dominates over lateral migration of the channel and beveling of the valley floor, limiting downstream valley widening despite increasing discharge. In the downstream limit, the channel eventually occupies the full valley floor, producing fully confined conditions where $w_v^* = 0$ (Fig. 3). In contrast, for the second end-member case, where valley widening outpaces channel widening (c=0.7, b=0.5) the channel progressively takes up a smaller and smaller fraction of the valley floor (Figure 2). As such, w_v^* generally increases downstream as the relative valley width increases. This end member is consistent with landscapes where lateral erosion is efficient relative to fluvial incision, such as in instances where abundant valley-bottom sediment cover acts to shield the channel floor from erosion and promote lateral channel migration (DeLisle & Yanites, 2023; Turowski, 2018). Under these conditions, downstream patterns in w_v^* predominately governed by relative valley width rather than relief generation and ridgeline topography.

Across both end-member cases, larger Erosion numbers, N_e, result in lower w_v^* and therefore more highly confined valleys (Fig. 3). This is because higher N_e reflects conditions that should produce more efficient vertical incision as predicted by SPIM, such as rapid tectonic uplift, weak bedrock, or increased precipitation. This enhanced erosional efficiency, summarized by high N_e, results in greater catchment relief and reduced w_v^*. High-N_e landscapes also tend to produce concave-up w_v^* profiles. Lower N_e values, reflective of landscapes with slower uplift, more resistant rocks, or more arid climates, result in high w_v^*, reflecting less confined valleys. Under these conditions, lateral erosion and valley widening overwhelm the topographic signature of relief such that w_v^* profiles become increasingly convex downstream, mirroring downstream increases in relative valley width (Fig. 1B). Taken together, these results suggest that under detachment-limited conditions, catchment-scale differences in w_v^* reflect

differences in the relative efficacy of vertical incision and lateral erosion as a function of variable uplift, erodibility, and precipitation, as summarized by the Erosion number, N_e.

3.2 Downstream valley confinement across King Range catchments

Across the seven King Range catchments, relative valley width systematically increases with decreasing Erosion Number, N_e (Figure 4A, R^2=0.69, Supplementary Information). This trend reflects downstream differences between valley- and channel-widening rates, expressed through the relative magnitudes of the w_v-A and w_c-A scaling exponents ($c - b$). The difference between these widening exponents is itself inversely proportional to N_e (R^2=0.41, see supplement). Six of the seven catchments exhibit positive $c - b$ values, indicating that valley widening outpaces channel widening downstream. The maximum difference ($c - b$ =0.13) occurs in Hardy Creek, the catchment with the lowest Erosion number (N_e =1.02 × 10^{-4}). In contrast, Kinsey Creek is the only catchment with a negative exponent difference ($c - b$=-0.06). Kinsey creek also has the second largest Erosion number (N_e=0.05). These differences strongly influence downstream patterns in relative valley width. For example, Juan Creek ($N_e = 2.89 \times 10^{-4}$, $c - b = 0.13$) exhibits nearly a 20-fold increase in relative valley width from headwaters to outlet, whereas relative valley width in Kinsey Creek increases by only a factor of two over the same downstream distance. Despite its negative $c - b$ value, valley-widening still outpaces channel-widening in the Kinsey Creek catchment due to differences in the coefficients of the previously reported scaling relationships (Snyder et al., 2003; Figure 4A, Supplementary Information).

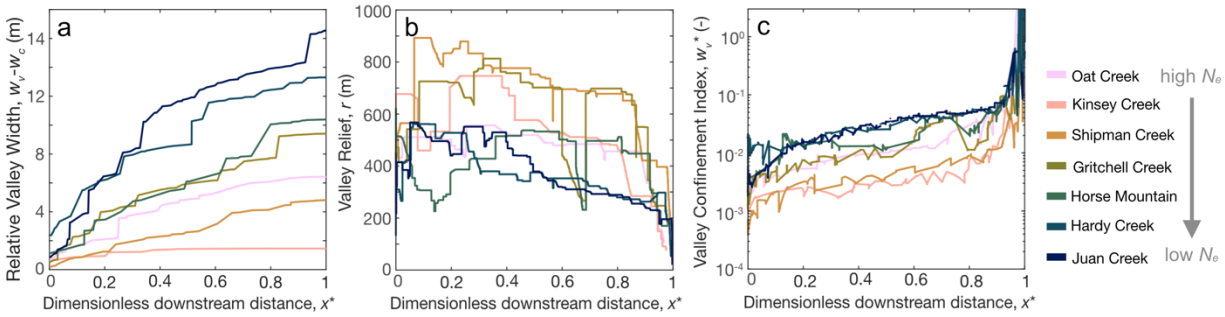

406
407 **Figure 4. A) Downstream profiles of relative valley width calculated from w_v-A and w_c-A**
408 **scaling reported in Snyder et al., (2003); B) Downstream profiles of catchment relief; C)**
409 **Downstream profiles in valley confinement index, w_v* derived from profiles in A and B.**
410
411 Catchment relief across the King range catchments similarly varies as a function of N_e
412 (Fig. 4B), such that catchments with larger N_e generally also exhibit higher catchment relief after
413 accounting for differences in the length of the main stem channel in each watershed (R^2=0.60,
414 Supplementary Information). Kinsey Creek, the catchment with the smallest relative valley width
415 is also the catchment with the maximum relative catchment relief, where r =746.5m (x_d =3.3
416 km, N_e =0.05). Juan Creek, the catchment with the largest relative valley width, also exhibits the
417 lowest relative catchment relief, r =567.3 m (x_d =11 km, N_e =2.89 × 10^{-4}).
418 These observed variations in relative valley width (Fig. 4A) and valley relief (Fig. 4B)
419 combine to produce systematic differences in w_v^* profiles across the study catchments (Fig. 4C).
420 All seven catchments are characterized by relatively narrow valleys and high relief, resulting in
421 generally low confinement index values (w_v^*=10^{-3}-10^{-1}). Despite the relative narrow range of w_v^*,
422 the resulting downstream profiles span a continuum from concave to convex (Fig. 4C) consistent
423 with the modeled behaviors described in Section 3.1 (Fig. 3). In all catchments, w_v^* increases
424 downstream, consistent with the end-member case in which valley widening outpaces channel
425 widening. This outcome is informed by differences in both the empirically-derived coefficients

and exponents of the channel width and valley width-drainage area scaling relationships reported by Snyder et al., (2003).

3.3 Model-data comparison of bedrock valley confinement profiles

Normalized median w_v* values for the King Range decrease as a function of increasing N_e (R^2=0.59, Fig. 5A), indicating that valleys become progressively more confined with increasing N_e. This decrease is well-captured by the modeled bedrock valley confinement profiles for the generalized Hack's Law scaling relationship $A=0.8L^{1.8}$ and SPIM exponents m=0.5, n=1, with a mean absolute error of MAE=0.13 between modeled and field-derived profiles. This parameterization is also broadly consistent with the best-fit SPIM exponents for the seven King Range catchments (m=0.43 and n=1; Snyder et al., 2003). The alternative parameterization ($A = 0.3L^2$, $m = 0.5$, $n = 2/3$) systematically underpredicts normalized median w_v^*, although the overall downstream trend with increasing N_e remains similar between the two model configurations. For all tested valley-width scaling exponents ($c = 0.2$–0.5), normalized median w_v^* profiles collapse (Fig. 5A). This indicates that while the choice of exponent does affect the catchment-average valley confinement, it does not influence the relative dependence of median w_v^* on N_e for a given parameter set after normalization. This is not necessarily surprising, since w_c-A scaling and w_v-A scaling are independent of N_e.

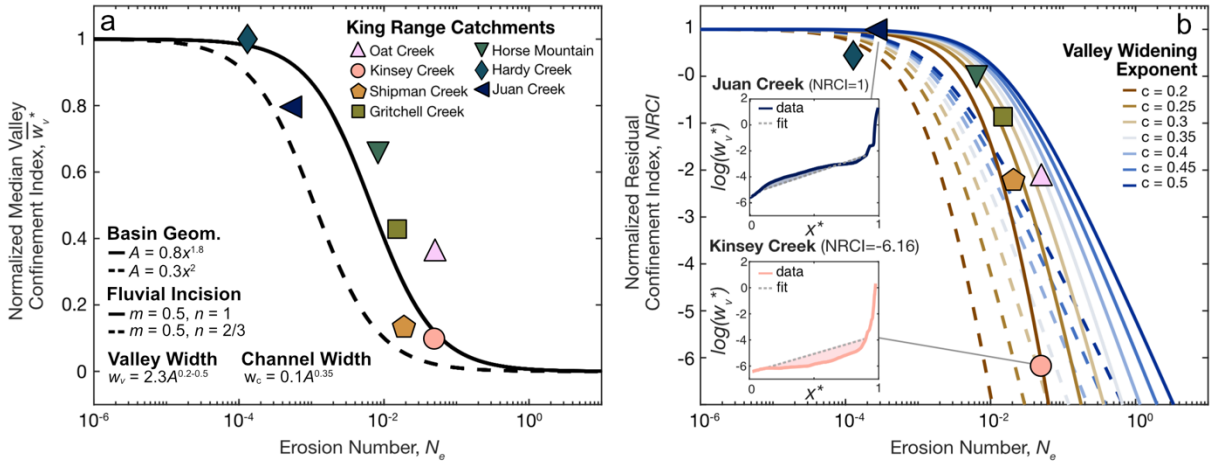

Figure 5. A) Normalized median w_v*, with varying N_e using two combinations of generalized basin geometry and stream power incision parameters (dashed and solid lines), w_v-A scaling exponents, c=0.2-0.5 (curves collapse), and channel width-drainage area scaling exponent, b=0.35, the average value for the King Range catchments. King Range values plotted as diamonds. B) Normalized residual confinement index, *NRCI* with varying N_e for the same scaling relationships used in A. King Range values plotted as diamonds. Insets show two w_v* profiles for two King Range catchments to illustrate differences in concavity informing their respective *NRCI* values (all catchment profiles included in Supplementary Information).

Normalized residual confinement index (*NRCI*) for the King Range catchments also decreases systematically as a function of increasing Erosion number as valley confinement profiles transition from convex to concave (R^2 = 0.73, Fig. 3, 4C, 5B). Four catchments exhibit negative *NRCI* values, indicative of concave confinement w_v* profiles. Kinsey Creek displays the minimum $NRCI$ value ($NRCI = -6.16$; Fig. 5B inset), consistent with its high N_e, narrow valleys, and large normalized relief described in Section 3.2. Taken together, these results indicate that the valley morphology of Kinsey Creek is likely governed by vertical incision

processes, such that the w_v* profile is strongly influenced by downstream patterns in catchment relief, and that these downstream patterns in relief are consistent with the formulation for interfluvial ridge height from Willet (2010). In contrast, three of the King Range catchments have positive $NRCI$ values, indicative of convex w_v* profiles. Juan Creek has the maximum convexity and resultant $NRCI = 1$, consistent with low N_e and observations of relatively wide valleys and low relative relief, as described in Section 3.2. Given this, we suggest that the valley morphology of Juan Creek is dominated by lateral erosion processes, at least compared to the other King Range catchments evaluated here, and that the downstream patterns in w_v* are primarily set by relative valley width rather than ridgeline topography. These contrasting end members suggest that the shape of w_v^* profiles across King Range catchments reflects a gradient in bedrock valley form more strongly dominated by incision-driven relief growth to those more strongly influenced by downstream valley widening.

The modeled profiles reproduce these observed $NRCI$ trends across the King Range well, particularly for the parameterization $A = 0.8L^{1.8}$, $m = 0.5$, and $n = 1$(Fig. 5B). However, unlike normalized median w_v*, the dependence of $NRCI$ on Erosion number is distinct for each valley width-drainage area scaling exponent, c. For a given N_e, relatively slow downstream valley widening rates, reflected by low values of c, produce increasingly negative *NRCI* and more concave profiles, reflecting relatively inefficient lateral erosion compared to vertical incision. Larger c values result in greater *NRCI* and more convex w_v* profiles as downstream valley-widening overwhelms relief generation via incision. Overall, c=0.3 provides the closest match to the relative NRCI values observed across the King Range catchments (MAE = 0.98). However, the absolute errors between each catchment and modeled w_v* profiles are minimized for different values of c (Supplementary Information). For example, the shape of the Kinsey Creek profile as

484 described by *NRCI*, is best described by the minimum model *c* value, *c*=0.2, and a difference in
485 valley and channel-drainage area scaling exponents of *c*-*b* = -0.15, consistent with the observed
486 *c*-*b* =-0.06. In contrast, Juan Creek, where reported *c*-*b*=0.13, is best described by the maximum
487 modeled *c* value, c=0.5, yielding a best-fit modeled *c*-*b*=0.15. Oat Creek, a catchment where
488 reported *c*-*b*=0.06, is best described by modeled profiles with *c*=0.35 (*c*-*b*=0). It is worth noting
489 here that exact agreement between observed and best-fit modeled *c* values is not expected
490 because the modeled profiles assume constant valley and channel width-drainage area scaling
491 coefficients. This assumption is not consistent with the observed scaling relationships reported
492 by Snyder et al., (2003) where both the coefficients and exponents of the derived drainage area
493 scaling relationships vary between catchments. Although additional calibration could likely
494 improve catchment-specific fits, the simplified framework captures the primary downstream
495 trends in bedrock valley morphology observed across the King Range catchments.

496 **5 Discussion and conclusions**

497 This contribution represents the first description of a steady-state expectation for
498 downstream patterns in bedrock valley morphology, as described by the downstream covariation
499 in valley width, channel width, and catchment relief, or the bedrock valley confinement index,
500 w_v*. The systematic differences observed in both the magnitude and shape of w_v^* profiles
501 ultimately reflect the relative efficacy of fluvial incision to lateral erosion. Within the framework
502 developed here, relief generation is governed entirely by detachment-limited bedrock incision,
503 which embeds the influence of climate, tectonics, and lithology through the application of the
504 SPIM (Willet, 2000). These combined influences are encapsulated in the Erosion number, N_e.
505 Comparison with the King Range catchments demonstrates that the simplified framework
506 developed here reproduces first-order variations in observed valley morphology across a gradient

507 in uplift and precipitation, suggesting that w_v^* profiles capture meaningful differences in valley
508 form linked to relative differences in incisional efficiency as described by SPIM and Ne.

509 In the model-data comparison presented here, modeled interfluvial ridge heights assume
510 that the only process that influences patterns in catchment relief is fluvial incision. For
511 detachment-limited landscapes, this assumption is generally appropriate (Whipple & Tucker,
512 1999; Willett, 2010) and here, is reinforced by the good agreement observed between modeled
513 w_v* profiles and w_v* for the King Range catchments (Fig. 3,4). However, in steep landscapes,
514 active landsliding may also act to limit catchment relief (e.g. Larsen & Montgomery, 2012),
515 modifying the relationship between fluvial incision and valley relief with knock-on
516 consequences for w_v*. Further, this enhanced hillslope sediment supply may result in valley floor
517 aggradation, further modifying the covariation between valley width and catchment relief as the
518 efficacy of fluvial incision is reduced and the valley becomes transport-limited (Clubb et al.,
519 2023; Shobe et al., 2018; Tofelde et al., 2022). However, even in transport-limited settings,
520 channel width, active valley width, and valley relief should still be expected to covary because
521 they remain dynamically linked through sediment transport and channel adjustment processes.
522 Indeed, previous studies have shown strong correlations between terrace height and valley width
523 across multiple cycles of aggradation and incision (Tofelde et al., 2022). Nevertheless, further
524 exploration is needed to assess the suitability of the framework developed here to these cases,
525 specifically the treatment of valley relief. At present, Willet (2010) provides the only general
526 formulation for expected downstream patterns in catchment relief.

527 It is worth emphasizing that the influence of climate, tectonics, and lithology on relative
528 valley width is not explicitly accounted for in the valley and channel width-drainage area scaling
529 relationships used here. While empirical evidence suggests that both valley and channel width-

drainage area scaling may be impacted by differences in climate, tectonics, and rock strength (Bufe et al., 2016; Clubb et al., 2023; Kostynick, Phillips, et al., 2026; Langston & Temme, 2019; Masteller et al., n.d.; Phillips et al., 2024; Tofelde et al., 2022), there is not yet a general framework capable of attributing differences in downstream scaling relationships to specific controls. This is likely because there remain remarkably few catchment-specific studies that constrain these scaling relationships, limiting cross-catchment comparisons. Perhaps more fundamentally, Snyder et al. remains one of the few studies to empirically constrain both channel-width and valley-width scaling relationships within the same set of catchments.We suggest that exploration of the variation of catchment specific scaling relationships for both valley and channel width, with Erosion number, N_e, may be a fruitful step forward towards explicitly accounting for these effects. Further, the application of process-based erosion models that combine vertical incision and lateral migration (e.g. Limaye and Lamb, 2014; Langston and Tucker, 2018; Turowski et al, 2024) may help identify the mechanisms driving systematic variations in downstream valley morphology. Ultimately, integrating detailed catchment-scale observations with transport-based frameworks for channel adjustment offers a path toward more physically grounded predictions of how river valleys respond to changing climate, uplift, sediment supply, and other perturbations.

The newly-developed modeling framework presented captures differences in bedrock valley morphology consistent with previous observations at individual valley cross-sections. Modeled decreases in overall valley confinement with increasing Erosion number are consistent with observations that valleys are typically relatively narrow in rapidly uplifting landscapes (Bufe et al., 2016, 2017) or in settings with less erodible bedrock (Langston & Temme, 2019; Schanz & Montgomery, 2016). These results are also consistent with process-based modeling

efforts (Limaye & Lamb, 2014). Beyond qualitative agreement with previous studies, the framework developed here captures systematic differences in valley morphology between King Range catchments spanning gradients in uplift and precipitation (Fig. 5, Snyder et al., 2003).

This contribution expands upon previous work by moving beyond a single cross section and instead considering the spatial covariation of valley width, channel width, and valley relief through a watershed from headwaters to outlet. The shape of confinement profiles varies systematically with Erosion number, providing a quantitative framework for distinguishing incision-dominated landscapes (concave profiles; negative *NRCI*) from those more strongly influenced by lateral valley widening (convex profiles; positive *NRCI*). It is worth noting that the model parameter space explored in this contribution is intentionally broad, aiming to capture the widest range of possible downstream trajectories in bedrock valley confinement. Further, the treatments of valley width, channel width, and catchment relief are fully independent within the preliminary exploration presented here. However, the tendency for the King Range catchments to cluster around a relatively limited range of modeled trajectories suggests that downstream valley morphology exhibits some degree of self-organization across catchments. This behavior is perhaps not surprising, as both valley width and catchment relief are generated through fluvial erosion, whereas the efficacy of fluvial erosion itself is fundamentally governed by water discharge, which is in turn embedded within downstream patterns in channel width. In this sense, downstream patterns in valley confinement reflect how channel width, valley width, and valley relief coevolve as a function of both catchment hydrology and erosion processes.

Beyond these catchment scale patterns, localized shifts in the relationship between elements of valley confinement index (relative valley width, relief) across a catchment may signal coincident shifts in the relative efficacy of vertical and lateral erosion processes that act to

set valley architecture locally and to identify downstream transitions with dominant valley-forming processes. This behavior is perhaps most clearly illustrated in Figure 3 for profiles with $c = 0.7$ and high N_e. In these cases, modeled confinement initially decreases in steep headwaters where the onset of fluvial incision rapidly generates catchment relief. Farther downstream, confinement reaches a minimum value and then begins to increase as downstream increases in valley width exceed downstream increases in relief. This transition suggests that lateral erosion and valley widening progressively exert a greater influence on valley morphology downstream. Along-river shifts in confinement trajectories may also reflect downstream changes in climatic, tectonic, or lithologic forcing. Gradual downstream changes may arise from orographic precipitation gradients (Forte & Rossi, 2024), whereas more punctuated transitions may reflect rivers traversing zones of enhanced uplift (Bufe et al., 2016) or more resistant bedrock (Langston & Temme, 2019).

Along-river variations in the threshold for sediment motion may provide an additional mechanism governing downstream transitions in bedrock valley confinement because sediment transport ultimately sets the relative efficacy of fluvial erosion. Sediment entrainment thresholds vary systematically with channel slope (Lamb et al., 2008; Prancevic & Lamb, 2015), the timing and magnitude of floods (Kostynick, et al., 2026; Masteller et al., 2019, 2025; Ockelford et al., 2019), riverbed structure and grain size distribution (Hodge et al., 2013; Kirchner et al., 1990; Masteller & Finnegan, 2017; Whitfield et al., 2025), and sediment supply (Dietrich et al., 1989; Hassan et al., 2020; Johnson, 2016). Because bedrock incision, and lateral channel migration are fundamentally governed by sediment transport, downstream variations in sediment mobility (Masteller et al., n.d.; Mueller et al., 2005) may systematically alter the relative efficacy of vertical incision and lateral erosion across a catchment. For example, enhanced thresholds for

599 motion in steep headwaters may suppress lateral channel mobility while maintaining efficient
600 vertical incision through impact-driven erosion. In contrast, downstream reductions in
601 entrainment thresholds may promote more persistent sediment mobility, enhancing lateral
602 channel migration and shifting valley evolution toward widening-dominated behavior. As such,
603 downstream confinement patterns may also reflect spatial variations in the efficiency with which
604 floods mobilize sediment and erode bedrock. Future work should focus on more explicitly
605 linking the relative efficacy of vertical and lateral erosion processes within a catchment and
606 downstream transitions in valley-forming processes under steady state conditions.

607 Recent advances in data availability and analysis tools position the community to
608 evaluate these relationships more systematically. The rapid expansion of publicly available,
609 high-resolution topographic datasets, combined with emerging tools for automated extraction of
610 channel width (e.g. Kostynick et al., 2026), valley width (e.g. Clubb et al., 2022), and valley
611 relief (e.g. Scherler & Schwanghart, 2020), now enables consistent, large-scale characterization
612 of river channel and valley geometry across diverse landscapes. Such analyses would not only
613 help constrain empirical drainage area scaling relationships for both channels and valleys but
614 also provide a pathway to more directly evaluate the controls on the covariation between these
615 elements of valley form, including the roles of climate, tectonics, and lithology. Future efforts in
616 these areas could allow for a more rigorous assessment of how natural systems populate the
617 model domain developed here, offering a means to test whether observed combinations of
618 scaling exponents align with steady-state expectations and to identify systematic deviations that
619 may reflect differences in process regime or transient landscape adjustment.

620 This study develops and tests a 1-D profile model capturing the downstream covariation
621 in valley width, channel width, and valley relief for detachment-limited landscapes under steady

state conditions. The modeling framework developed here combines scaling relationships for channel width and valley width with downstream trends in valley relief generated via fluvial incision to produce longitudinal profiles in bedrock valley confinement, w_v *, for a range of erosional efficiencies, summarized by the Erosion number, N_e, which captures the combined effects of tectonics, climate, and lithology on fluvial incision and relief generation. We find systematic variations in modeled w_v* with increasing N_e that are in good agreement with bedrock valley confinement profiles from catchments in the King Range, CA (Snyder et al., 2003). We suggest that the framework presented here serves as a robust steady-state expectation, or null hypothesis, that can be used to compare differences in bedrock valley morphology more directly across settings and to attribute observed differences in valley morphologic to specific drivers.

Table 2. Parameter Values and Units

Basic Variables	
x (m)	Downstream distance from channel head
x_d (m)	Maximum downstream distance
x_*	Dimensionless downstream distance
A (m^2)	drainage area
Q (m^3/s)	water discharge
w_c (m)	channel width
w_v (m)	valley width
r (m)	valley relief
w_{v*}	bedrock valley confinement index
S	channel gradient
E (m/yr)	channel incision rate
U (m/yr)	rock uplift rate
P (m/yr)	precipitation rate
K (1-2m/yr, where m is a drainage area-scaling exponent)	Coefficient of erosion
N_e	Erosion Number
Scaling parameters	
k_c (m^{1-2b})	channel width-drainage area coefficient
b	channel width-drainage area exponent

k_v (m^{1-2c})	valley width-drainage area coefficient
c	valley width-drainage area exponent
k_r ($m^{2-1/h}$)	Hack's law scaling coefficient
h	Hack's law scaling exponent
m	SPIM drainage area exponent
n	SPIM slope exponent

Acknowledgments

The author thanks Jedidiah Dale and Rachel Glade for helpful discussions.

Availability Statement

Topographic data used in this study are available from the U.S. Geological Survey, National Geospatial Program. USGS 3DEP lidar data was downloaded from OpenTopography (https://www.opentopography.org/). All figures utilize perceptually uniform *scientific colourmaps*. All data used to create the figures referenced in the text are included as part of the supplementary information. Supplemental code is available at https://zenodo.org/records/20061114?preview=1&token=eyJhbGciOiJIUzUxMiJ9.eyJpZCI6Ijc3NTkxNTVhLTJkNWItNGRlNy04Y2M2LTNlMTZiYzc4NjA4MiIsImRhdGEiOnt9LCJyYW5kb20iOiI1MTMyZTk1NjExZTk3YzE4NTdmNDUyYjdiNTg5NDJkNCJ9.oO_MeRk9DpqAHSUSBThTHSpw79Tfz5ndRT62oOwflIxsERe4uAdxubZv9JCL76YLHyOEldKqvlqc5hNQfAvliw. A note to editors and reviewers: *The final formally published reposotpru will be cited here with a DOI following review. The delay is to enable edits to the dataset if methodological changes are suggested during the review process that would result in material changes to the data.*

Conflict of Interest Disclosure

The author declares no conflicts of interests.

References

Allmendinger, N. E., Pizzuto, J. E., Potter, N., Johnson, T. E., & Hession, W. C. (2005). The influence of riparian vegetation on stream width, eastern Pennsylvania, USA. *Geological Society of America Bulletin*, *117*(1–2), 229–243. https://doi.org/10.1130/B25447.1

Anderson, R. J., Bledsoe, B. P., & Hession, W. C. (2004). Width of Streams and Rivers in Response to Vegetation, Bank Material, and Other Factors. *JAWRA Journal of the American Water Resources Association*, *40*(5), 1159–1172. https://doi.org/10.1111/j.1752-1688.2004.tb01576.x

Beeson, H. W., Flitcroft, R. L., Fonstad, M. A., & Roering, J. J. (2018). Deep-Seated Landslides Drive Variability in Valley Width and Increase Connectivity of Salmon Habitat in the Oregon Coast Range. *JAWRA Journal of the American Water Resources Association*, *54*(6), 1325–1340. https://doi.org/10.1111/1752-1688.12693

Brocard, G. Y., & van der Beek, P. A. (2006). Influence of incision rate, rock strength, and bedload supply on bedrock river gradients and valley-flat widths: Field-based evidence and calibrations from western Alpine rivers (southeast France). In S. D. Willett, N. Hovius, M. T. Brandon, & D. M. Fisher, *Tectonics, Climate, and Landscape Evolution*. Geological Society of America. https://doi.org/10.1130/2006.2398(07)

Bufe, A., Paola, C., & Burbank, D. W. (2016). Fluvial bevelling of topography controlled by lateral channel mobility and uplift rate. *Nature Geoscience*, *9*(9), 706–710. https://doi.org/10.1038/ngeo2773

Bufe, A., Burbank, D. W., Liu, L., Bookhagen, B., Qin, J., Chen, J., et al. (2017). Variations of Lateral Bedrock Erosion Rates Control Planation of Uplifting Folds in the Foreland of the Tian Shan, NW China. *Journal of Geophysical Research: Earth Surface*, *122*(12), 2431–2467. https://doi.org/10.1002/2016JF004099

Bursztyn, N., Pederson, J. L., Tressler, C., Mackley, R. D., & Mitchell, K. J. (2015). Rock strength along a fluvial transect of the Colorado Plateau – quantifying a fundamental control on geomorphology. *Earth and Planetary Science Letters*, *429*, 90–100. https://doi.org/10.1016/j.epsl.2015.07.042

Chen, S.-A., Michaelides, K., Grieve, S. W. D., & Singer, M. B. (2019). Aridity is expressed in river topography globally. *Nature*, *573*(7775), 573–577. https://doi.org/10.1038/s41586-019-1558-8

Clubb, F. J., Weir, E. F., & Mudd, S. M. (2022). Continuous measurements of valley floor width in mountainous landscapes. *Earth Surface Dynamics*, *10*(3), 437–456. https://doi.org/10.5194/esurf-10-437-2022

Clubb, F. J., Mudd, S. M., Schildgen, T. F., van der Beek, P. A., Devrani, R., & Sinclair, H. D. (2023). Himalayan valley-floor widths controlled by tectonically driven exhumation. *Nature Geoscience*, *16*(8), 739–746. https://doi.org/10.1038/s41561-023-01238-8

681 DeLisle, C., & Yanites, B. J. (2023). Rethinking Variability in Bedrock Rivers: Sensitivity of Hillslope Sediment
682 Supply to Precipitation Events Modulates Bedrock Incision During Floods. *Journal of Geophysical*
683 *Research: Earth Surface*, *128*(9), e2023JF007148. https://doi.org/10.1029/2023JF007148
684 Dietrich, W. E., Kirchner, J. W., Ikeda, H., & Iseya, F. (1989). Sediment supply and the development of the coarse
685 surface layer in gravel-bedded rivers. *Nature*, *340*(6230), 215–217. https://doi.org/10.1038/340215a0
686 Duvall, A. (2004). Tectonic and lithologic controls on bedrock channel profiles and processes in coastal California.
687 *Journal of Geophysical Research*, *109*(F3), F03002. https://doi.org/10.1029/2003JF000086
688 Ferguson, R. I. (1986). Hydraulics and hydraulic geometry. *Progress in Physical Geography: Earth and*
689 *Environment*, *10*(1), 1–31. https://doi.org/10.1177/030913338601000101
690 Ferrier, K. L., Huppert, K. L., & Perron, J. T. (2013). Climatic control of bedrock river incision. *Nature*, *496*(7444),
691 206–209. https://doi.org/10.1038/nature11982
692 Finnegan, N. J., & Balco, G. (2013). Sediment supply, base level, braiding, and bedrock river terrace formation:
693 Arroyo Seco, California, USA. *Geological Society of America Bulletin*, *125*(7–8), 1114–1124.
694 https://doi.org/10.1130/B30727.1
695 Finnegan, N. J., Hallet, B., Montgomery, D. R., Zeitler, P. K., Stone, J. O., Anders, A. M., & Yuping, L. (2008).
696 Coupling of rock uplift and river incision in the Namche Barwa-Gyala Peri massif, Tibet. *Geological*
697 *Society of America Bulletin*, *120*(1–2), 142–155. https://doi.org/10.1130/B26224.1
698 Forte, A. M., & Rossi, M. W. (2024). Stochastic in Space and Time: 2. Effects of Simulating Orographic Gradients
699 in Daily Runoff Variability on Bedrock River Incision. *Journal of Geophysical Research: Earth Surface*,
700 *129*(3), e2023JF007327. https://doi.org/https://doi.org/10.1029/2023JF007327
701 Gleason, C. J. (2015). Hydraulic geometry of natural rivers: A review and future directions. *Progress in Physical*
702 *Geography: Earth and Environment*, *39*(3), 337–360. https://doi.org/10.1177/0309133314567584
703 Hack, J. (1957). Studies of longitudinal stream profiles in Virginia and Maryland. Retrieved January 5, 2024, from
704 https://pubs.usgs.gov/publication/pp294B
705 Hancock, G. S., & Anderson, R. S. (2002). Numerical modeling of fluvial strath-terrace formation in response to
706 oscillating climate. *GSA Bulletin*, *114*(9), 1131–1142. https://doi.org/10.1130/0016-
707 7606(2002)114%3C1131:NMOFST%3E2.0.CO;2

Hassan, M. A., Saletti, M., Johnson, J. P. L., Ferrer-Boix, C., Venditti, J. G., & Church, M. (2020). Experimental Insights Into the Threshold of Motion in Alluvial Channels: Sediment Supply and Streambed State. *Journal of Geophysical Research: Earth Surface*, *125*(12), e2020JF005736. https://doi.org/10.1029/2020JF005736

He, X., Yuan, X., He, C., Clubb, F. J., & Shen, X. (2026). Climate-Driven Strath Terrace Formation Revealed by a Fluvial Erosion-Deposition Model Considering Channel Widths. *Journal of Geophysical Research: Earth Surface*, *131*(1), e2025JF008594. https://doi.org/10.1029/2025JF008594

Hodge, R. A., Sear, D. A., & Leyland, J. (2013). Spatial variations in surface sediment structure in riffle-pool sequences: a preliminary test of the Differential Sediment Entrainment Hypothesis (DSEH): Spatial Variations in Sediment Structure in Riffle-Pool Sequences. *Earth Surface Processes and Landforms*, *38*(5), 449–465. https://doi.org/10.1002/esp.3290

Howard, A. D. (1994). A detachment-limited model of drainage basin evolution. *Water Resources Research*, *30*(7), 2261–2285. https://doi.org/10.1029/94WR00757

Johnson, J. P. L. (2016). Gravel threshold of motion: a state function of sediment transport disequilibrium? *Earth Surface Dynamics*, *4*(3), 685–703. https://doi.org/10.5194/esurf-4-685-2016

Keen-Zebert, A., Hudson, M. R., Shepherd, S. L., & Thaler, E. A. (2017). The effect of lithology on valley width, terrace distribution, and bedload provenance in a tectonically stable catchment with flat-lying stratigraphy. *Earth Surface Processes and Landforms*, *42*(10), 1573–1587. https://doi.org/10.1002/esp.4116

Kirby, E., & Whipple, K. X. (2012). Expression of active tectonics in erosional landscapes. *Journal of Structural Geology*, *44*, 54–75. https://doi.org/10.1016/j.jsg.2012.07.009

Kirchner, J. W., Dietrich, W. E., Iseya, F., & Ikeda, H. (1990). The variability of critical shear stress, friction angle, and grain protrusion in water-worked sediments. *Sedimentology*, *37*(4), 647–672. https://doi.org/https://doi.org/10.1111/j.1365-3091.1990.tb00627.x

Kostynick, R. P., Phillips, C. B., & Masteller, C. C. (2026). High-Resolution Channel Geometry Reveals Contrasting Styles of Gravel River Adjustment. *Geophysical Research Letters*. https://doi.org/10.1029/2025GL118412

Kostynick, R. P., Prata, J., Bower, J., & Masteller, C. C. (2026). Slope-dependent riverbed strengthening and the evolution of the threshold for motion in gravel-bed rivers. Retrieved from https://eartharxiv.org/repository/view/12091/

Lamb, M. P., Dietrich, W. E., & Venditti, J. G. (2008). Is the critical Shields stress for incipient sediment motion dependent on channel-bed slope? *Journal of Geophysical Research*, *113*(F2), F02008. https://doi.org/10.1029/2007JF000831

Langston, A. L., & Robertson, C. H. (2023). Wide bedrock valley development and sensitivity to environmental perturbations: Insights from flume experiments in erodible bedrock. *Earth Surface Processes and Landforms*, *48*(15), 3041–3058. https://doi.org/10.1002/esp.5680

Langston, A. L., & Temme, A. J. A. M. (2019). Impacts of Lithologically Controlled Mechanisms on Downstream Bedrock Valley Widening. *Geophysical Research Letters*, *46*(21), 12056–12064. https://doi.org/10.1029/2019GL085164

Langston, A. L., & Tucker, G. E. (2018). Developing and exploring a theory for the lateral erosion of bedrock channels for use in landscape evolution models. *Earth Surface Dynamics*, *6*(1), 1–27. https://doi.org/10.5194/esurf-6-1-2018

Larsen, I. J., & Montgomery, D. R. (2012). Landslide erosion coupled to tectonics and river incision. *Nature Geoscience*, *5*(7), 468–473. https://doi.org/10.1038/ngeo1479

Leopold, L. B., & Maddock, T. (1953). The Hydraulic Geometry of Stream Channels and Some Physiographic Implications. *U.S. Geological Survey Professional Paper*, *252*. https://doi.org/10.3133/pp252

Limaye, A. B. S., & Lamb, M. P. (2014). Numerical simulations of bedrock valley evolution by meandering rivers with variable bank material. *Journal of Geophysical Research: Earth Surface*, *119*(4), 927–950. https://doi.org/10.1002/2013JF002997

MACKIN, J. H. (1937). Erosional history of the Big Horn Basin, Wyoming. *GSA Bulletin*, *48*(6), 813–894. https://doi.org/10.1130/GSAB-48-813

Malatesta, L. C., Prancevic, J. P., & Avouac, J.-P. (2017). Autogenic entrenchment patterns and terraces due to coupling with lateral erosion in incising alluvial channels. *Journal of Geophysical Research: Earth Surface*, *122*(1), 335–355. https://doi.org/10.1002/2015JF003797

Masteller, C.C., & Finnegan, N. J. (2017). Interplay between grain protrusion and sediment entrainment in an experimental flume. *Journal of Geophysical Research: Earth Surface*, *122*(1), 274–289. https://doi.org/10.1002/2016JF003943

763 Masteller, Claire C., Finnegan, N. J., Turowski, J. M., Yager, E. M., & Rickenmann, D. (2019). History-Dependent
764 Threshold for Motion Revealed by Continuous Bedload Transport Measurements in a Steep Mountain
765 Stream. *Geophysical Research Letters*, *46*(5), 2583–2591. https://doi.org/10.1029/2018GL081325
766 Masteller, Claire C., Johnson, J. P. L., Rickenmann, D., & Turowski, J. M. (2025). Modeling memory in gravel-bed
767 rivers: a flow-history-dependent relation for evolving thresholds of motion. *Earth Surface Dynamics*, *13*(4),
768 593–605. https://doi.org/10.5194/esurf-13-593-2025
769 Masteller, Claire C., Phillips, C. B., Kostynick, R. P., Castejon-Villalobos, J. F., Lopez, C. G., Shallue, M. K., et al.
770 (n.d.). Tracking the trajectory of alluvial channel adjustment along a river's profile. Retrieved from
771 https://www.authorea.com/users/721760/articles/1389848-tracking-the-trajectory-of-alluvial-channel-
772 adjustment-along-a-river-s-profile?commit=6b8c3cfa541fa066011c7bd093ab3cbce4fe7c62
773 May, C., Roering, J., Eaton, L. S., & Burnett, K. M. (2013). Controls on valley width in mountainous landscapes:
774 The role of landsliding and implications for salmonid habitat. *Geology*, *41*(4), 503–506.
775 https://doi.org/10.1130/G33979.1
776 Merritts, D., & Bull, W. B. (1989). Interpreting Quaternary uplift rates at the Mendocino triple junction, northern
777 California, from uplifted marine terraces. *Geology*, *17*(11), 1020. https://doi.org/10.1130/0091-
778 7613(1989)017%3C1020:IQURAT%3E2.3.CO;2
779 Métivier, F., Lajeunesse, E., & Devauchelle, O. (2017). Laboratory rivers: Lacey's law, threshold theory, and
780 channel stability. *Earth Surface Dynamics*, *5*(1), 187–198. https://doi.org/10.5194/esurf-5-187-2017
781 Montgomery, D. R., & Dietrich, W. E. (1992). Channel initiation and the problem of landscape scale. *Science (New*
782 *York, N.Y.)*, *255*(5046), 826–830. https://doi.org/10.1126/science.255.5046.826
783 Montgomery, David R. (2002). Valley formation by fluvial and glacial erosion. *Geology*, *30*(11), 1047–1050.
784 https://doi.org/10.1130/0091-7613(2002)030%3C1047:VFBFAG%3E2.0.CO;2
785 Montgomery, David R, & Brandon, M. T. (2002). Topographic controls on erosion rates in tectonically active
786 mountain ranges. *Earth and Planetary Science Letters*, *201*(3), 481–489. https://doi.org/10.1016/S0012-
787 821X(02)00725-2
788 Montgomery, David R., & Gran, K. B. (2001). Downstream variations in the width of bedrock channels. *Water*
789 *Resources Research*, *37*(6), 1841–1846. https://doi.org/10.1029/2000WR900393

790 Moody, J. A., & Troutman, B. M. (2002). Characterization of the spatial variability of channel morphology. *Earth*
791 *Surface Processes and Landforms*, *27*(12), 1251–1266. https://doi.org/10.1002/esp.403
792 Mueller, E. R., Pitlick, J., & Nelson, J. M. (2005). Variation in the reference Shields stress for bed load transport in
793 gravel-bed streams and rivers. *Water Resources Research*, *41*(4).
794 Ockelford, A., Woodcock, S., & Haynes, H. (2019). The impact of inter-flood duration on non-cohesive sediment
795 bed stability. *Earth Surface Processes and Landforms*, *44*(14), 2861–2871.
796 https://doi.org/10.1002/esp.4713
797 Ortega-Becerril, J. A., Garzón, G., Tejero, R., Meriaux, A.-S., Delunel, R., Merchel, S., & Rugel, G. (2018).
798 Controls on strath terrace formation and evolution: The lower Guadiana River, Pulo do Lobo, Portugal.
799 *Geomorphology*, *319*, 62–77. https://doi.org/10.1016/j.geomorph.2018.07.015
800 Pazzaglia, F. J., & Brandon, M. T. (2001). A Fluvial Record of Long-term Steady-state Uplift and Erosion Across
801 the Cascadia Forearc High, Western Washington State. *American Journal of Science*, *301*(4–5), 385–431.
802 https://doi.org/10.2475/ajs.301.4-5.385
803 Phillips, C. B., Masteller, C. C., Blaylock, J., Van Iwaarden, F., & Johnson, J. P. L. (2024). Variability in River
804 Width Reveals Climatic Influence on Channel Geometry. *Geophysical Research Letters*, *51*(23),
805 e2024GL111789. https://doi.org/10.1029/2024GL111789
806 Phillips, Colin B., Masteller, C. C., Slater, L. J., Dunne, K. B. J., Francalanci, S., & Lanzoni, S. (2022). Threshold
807 constraints on the size, shape and stability of alluvial rivers. *Nature Reviews Earth & Environment*, 1–14.
808 https://doi.org/10.1038/s43017-022-00282-z
809 Prancevic, J. P., & Lamb, M. P. (2015). Particle friction angles in steep mountain channels. *Journal of Geophysical*
810 *Research: Earth Surface*, *120*(2), 242–259. https://doi.org/10.1002/2014JF003286
811 Rigon, R., Rodriguez-Iturbe, I., Maritan, A., Giacometti, A., Tarboton, D. G., & Rinaldo, A. (1996). On Hack's
812 Law. *Water Resources Research*, *32*(11), 3367–3374. https://doi.org/10.1029/96WR02397
813 Schanz, S. A., & Montgomery, D. R. (2016). Lithologic controls on valley width and strath terrace formation.
814 *Geomorphology*, *258*, 58–68. https://doi.org/10.1016/j.geomorph.2016.01.015
815 Schanz, S. A., Montgomery, D. R., & Collins, B. D. (2019). Anthropogenic strath terrace formation caused by
816 reduced sediment retention. *Proceedings of the National Academy of Sciences*, *116*(18), 8734–8739.
817 https://doi.org/10.1073/pnas.1814627116

818 Scherler, D., & Schwanghart, W. (2020). Drainage divide networks – Part 1: Identification and ordering in digital
819 elevation models. *Earth Surface Dynamics*, *8*(2), 245–259. https://doi.org/10.5194/esurf-8-245-2020
820 Schwanghart, W., & Scherler, D. (2014). Short Communication: TopoToolbox 2 – MATLAB-based software for
821 topographic analysis and modeling in Earth surface sciences. *Earth Surface Dynamics*, *2*(1), 1–7.
822 https://doi.org/10.5194/esurf-2-1-2014
823 Shobe, C. M., Tucker, G. E., & Rossi, M. W. (2018). Variable-Threshold Behavior in Rivers Arising From
824 Hillslope-Derived Blocks. *Journal of Geophysical Research: Earth Surface*, *123*(8), 1931–1957.
825 https://doi.org/10.1029/2017JF004575
826 Snyder, N. P. (2000). Landscape response to tectonic forcing: Digital elevation model analysis of stream profiles in
827 the Mendocino triple junction region, northern California. *Geological Society of America Bulletin*.
828 Snyder, N. P., Whipple, K. X., Tucker, G. E., & Merritts, D. J. (2003). Channel response to tectonic forcing: field
829 analysis of stream morphology and hydrology in the Mendocino triple junction region, northern California.
830 *Geomorphology*, *53*(1–2), 97–127.
831 Tofelde, S., Bufe, A., & Turowski, J. M. (2022). Hillslope Sediment Supply Limits Alluvial Valley Width. *AGU*
832 *Advances*, *3*(6), e2021AV000641. https://doi.org/10.1029/2021AV000641
833 Tomkin, J. H., Brandon, M. T., Pazzaglia, F. J., Barbour, J. R., & Willett, S. D. (2003). Quantitative testing of
834 bedrock incision models for the Clearwater River, NW Washington State: QUANTITATIVE TESTING OF
835 RIVER INCISION MODELS. *Journal of Geophysical Research: Solid Earth*, *108*(B6).
836 https://doi.org/10.1029/2001JB000862
837 Turowski, J. M. (2018). Alluvial cover controlling the width, slope and sinuosity of bedrock channels. *Earth Surface*
838 *Dynamics*, *6*(1), 29–48. https://doi.org/10.5194/esurf-6-29-2018
839 Turowski, J. M., Bufe, A., & Tofelde, S. (2024). A physics-based model for fluvial valley width. *Earth Surface*
840 *Dynamics*, *12*(2), 493–514. https://doi.org/10.5194/esurf-12-493-2024
841 Van Appledorn, M., Baker, M. E., & Miller, A. J. (2019). River-valley morphology, basin size, and flow-event
842 magnitude interact to produce wide variation in flooding dynamics. *Ecosphere*, *10*(1), e02546.
843 https://doi.org/10.1002/ecs2.2546

Wegmann, K. W., & Pazzaglia, F. J. (2002). Holocene strath terraces, climate change, and active tectonics: The Clearwater River basin, Olympic Peninsula, Washington State. *GSA Bulletin*, *114*(6), 731–744. https://doi.org/10.1130/0016-7606(2002)114%3C0731:HSTCCA%3E2.0.CO;2

Whipple, K. X. (2004). BEDROCK RIVERS AND THE GEOMORPHOLOGY OF ACTIVE OROGENS. *Annual Review of Earth and Planetary Sciences*, *32*(1), 151–185. https://doi.org/10.1146/annurev.earth.32.101802.120356

Whipple, K. X., & Tucker, G. E. (1999). Dynamics of the stream-power river incision model: Implications for height limits of mountain ranges, landscape response timescales, and research needs. *Journal of Geophysical Research: Solid Earth*, *104*(B8), 17661–17674. https://doi.org/10.1029/1999JB900120

Whitbread, K., Jansen, J., Bishop, P., & Attal, M. (2015). Substrate, sediment, and slope controls on bedrock channel geometry in postglacial streams: POSTGLACIAL CHANNEL GEOMETRY. *Journal of Geophysical Research: Earth Surface*, *120*(5), 779–798. https://doi.org/10.1002/2014JF003295

Whitfield, D., Baynes, E. R. C., Hodge, R. A., Rice, S. P., & Yager, E. M. (2025). The Influence of Gravel-Bed Structure on Grain Mobility Thresholds: Comparison of Force-Balance Approaches. *Journal of Geophysical Research: Earth Surface*, *130*(5), e2025JF008333. https://doi.org/10.1029/2025JF008333

Willett, S. D. (1999). Orogeny and orography: The effects of erosion on the structure of mountain belts. *Journal of Geophysical Research: Solid Earth*, *104*(B12), 28957–28981. https://doi.org/10.1029/1999JB900248

Willett, S. D. (2010). Erosion on a line. *Tectonophysics*, *484*(1), 168–180. https://doi.org/10.1016/j.tecto.2009.09.011

Wobus, C., Whipple, K. X., Kirby, E., Snyder, N., Johnson, J., Spyropolou, K., et al. (2006). Tectonics from topography: Procedures, promise, and pitfalls. In S. D. Willett, N. Hovius, M. T. Brandon, & D. M. Fisher (Eds.), *Tectonics, Climate, and Landscape Evolution* (Vol. 398, p. 0). Geological Society of America. https://doi.org/10.1130/2006.2398(04)

Wohl, E. (2004). Limits of downstream hydraulic geometry. *Geology*, *32*(10), 897. https://doi.org/10.1130/G20738.1

Wohl, E. (2008). The effect of bedrock jointing on the formation of straths in the Cache la Poudre River drainage, Colorado Front Range. *Journal of Geophysical Research: Earth Surface*, *113*(F1). https://doi.org/10.1029/2007JF000817

Wohl, E., & David, G. C. L. (2008). Consistency of scaling relations among bedrock and alluvial channels. *Journal of Geophysical Research: Earth Surface*, *113*(F4). https://doi.org/10.1029/2008JF000989

Zondervan, J. R., Stokes, M., Boulton, S. J., Telfer, M. W., Mather, A. E., & Belfoul, M. A. (2024). Lithological controls on the timing of strath terrace staircase formation in a collisional mountain belt. *Earth Surface Processes and Landforms*, *49*(7), 2134–2154. https://doi.org/10.1002/esp.5821

JGR-Earth Surface

Supporting Information for

Downstream patterns in bedrock valley morphology encode climatic and tectonic forcing

C.C. Masteller[1]

[1]Department of Earth, Environmental, and Planetary Sciences, Washington University in St. Louis.

Contents of this file

Additional Supporting Information (Files uploaded separately)

DS1. Excel spreadsheet of supplementary datasets, full model output, and data-model comparison

Introduction

The supplemental information provides supporting details regarding:

- T1: Details regarding the calculation of interfluvial ridge heights and erosion numbers used in this study
- Fig. S1: c-b versus erosion number for King Range catchments
- Fig. S2: Modeled median wv* values and normalized median wv* values for varying valley widening coefficient, kv, and constant valley widening exponent, c
- Fig. S3: Modeled median wv* values and normalized median wv* values for constant valley widening coefficient, kv, and variable valley widening exponent, c (Fig. 4a)
- Fig. S4: wv* profiles and associated calculations of RCI and NRCI for all King Range catchments.

Text S1.

Modeling interfluvial ridge height

Downstream profiles of interfluvial ridge height are calculated following the analytical framework developed by Willett (2010), which combines the stream power incision model (SPIM) with Hack's Law to derive expected steady-state ridge elevations as a function of downstream distance. Under steady-state conditions, bedrock incision rate equals rock uplift rate ($E = U$), such that the channel longitudinal profile can be solved analytically from the SPIM. The non-dimensional channel elevation profile is first obtained by integrating the steady-state form of the SPIM (Equation 7 in Willett, 2010), yielding a solution for dimensionless channel elevation z^* as a function of dimensionless downstream position x^* (Equation 8 in Willett, 2010). Interfluvial ridge height emerges from recognizing that tributary channels, which drain perpendicular to the main stem, follow the same SPIM solution when scaled by their own length in the cross-stream (y) direction using Hack's Law. Substituting tributary length y for downstream distance x, and scaling by x_d, yields the total relief for a tributary channel — equivalent to the interfluvial ridge height at position x*, given by Equation 10 of Willett (2010), as follows:

$$z_d^* = y_c^* \tan\,\theta_c + y_d^{*(1-hm/n)} N_e \left(\frac{1}{1-hm/n}\right)\left(1-\left(\frac{y_c^*}{y_d^*}\right)^{(1-hm/n)}\right), \frac{hm}{n} \neq 1$$

$$z_d^* = y_c^* \tan\,\theta_c - N_e \ln\left(\frac{y_c^*}{y_d^*}\right), \frac{hm}{n} = 1$$

where y^*_c and y^*_d are the dimensionless channel head position and tributary length respectively, θ_c is the channel head gradient, and N_e is the Erosion number (Equation 6 in Willett, 2010; Equation 6 in this study). The shape of the resulting ridge profile is governed by the exponent hm/n, such that when $hm/n < 1$ the ridge profile is concave, whereas when $hm/n > 1$ the profile becomes convex, producing greater relief at intermediate distances from the divide. The Erosion number N_e scales the overall magnitude of ridge height, such that higher N_e amplifies relief throughout the catchment, while lower N_e suppresses it, producing the relatively open, low-relief valleys characteristic of slowly uplifting or more resistant landscapes.

Erosion Number versus Uplift-Erosion Number

Similar to the Erosion Number, the Uplift-Erosion Number presented in (Whipple & Tucker, 1999) can summarize relative differences in uplift, precipitation, and erodibility. The Uplift-Erosion number also includes a vertical length scale, typically some measure of relief, to account for vertical differences in scale between catchments in addition to differences in stream length. We also calculated the Uplift-Erosion number for the King Range study catchments using the maximum catchment relief. We found that while there were differences in Ne and the Uplift-Erosion number due to the introduction of an additional scalar, that the Erosion Number and the Uplift-Erosion

number remained strongly correlated across the study catchments. Thus, to be consistent with the formulation for interfluvial ridge height in Willet (2010), we use the calculated Erosion numbers in this study. Calculated Uplift-Erosion numbers are included in the supplementary Excel spreadsheet.

Influence of precipitation

There is an orographically-driven precipitation gradient across the study sites, with P~0.5 m/yr from the two southernmost catchments and P~3 m/yr in the five northern catchments. It is worth noting here that the orographic precipitation effect described above may also be embedded in catchment-specific erodibility (Ferrier et al., 2013 among others). Indeed, Snyder attributes differences in their derived K values to this effect. Given this, precipitation effects can be incorporated into Ne both directly in P and indirectly in K, which may further enhance differences between catchments. Using a median value for precipitation to calculate Ne across all catchments resulted in an average percent difference of about 2% in calculated erosion numbers when compared to use of a spatially variable P. Given this, we conclude that while there is some imprint of orographic precipitation effects on erodibility, in this case Ne is not strongly influenced by doubly accounting for this effect in both K and P. Given this, we use a spatially variable P when calculating Ne in this study.

Determination of Hack's Law

We found systematic decreases in Topotoolbox-derived Hack's Law exponents with increasing Ne. In addition, we determine best-fit coefficients for Hack's Law scaling relationships with fixed exponents of h=1.8 and h=2 to more directly compare to the generalized models that we developed. These relationships resulted in slightly different Erosion Numbers for the King Range catchments but did not fundamentally change the results. Given this, we selected the Erosion Numbers calculated from our Topotoolbox-derived Hack's Law values because these resulted in the best fit to data. We report the Erosion Numbers calculated using best-fit coefficients for fixed exponents of h=1.8 and h=2 in the supplementary Excel spreadsheet.

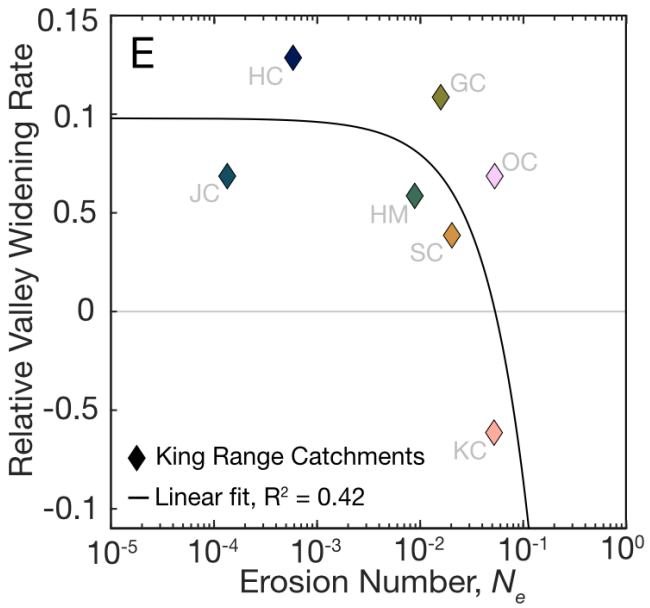

Figure S1. Difference between wv-A and wc-A scaling exponents, c and b, with calculated erosion number for King Range Catchments (Snyder et al., 2003).

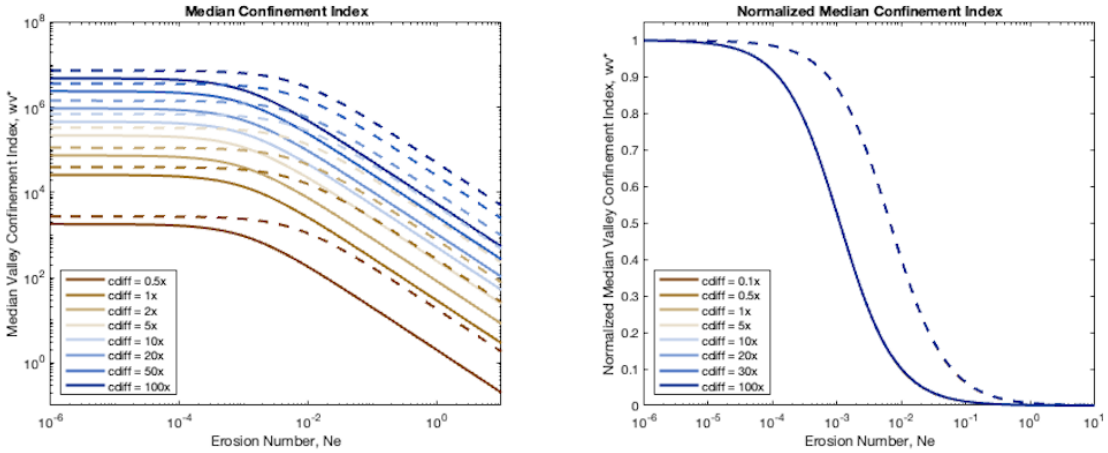

Figure S2. Modeled median wv* values and normalized median wv* values for varying valley widening coefficient, kv, and constant valley widening exponent, c=0.5, which is equivalent to specified channel widening exponent, b=0.5. the range of kv coefficinents explored varied from 0.5 times the channel widening coefficient, kw, to 100 times the channel widening coefficient, kw. Dashed and solid lines relate to two combinations of

Hack's Law Scaling and SPIM parameterizations, $A=0.3L^2$, $m=0.5$, and $n=2/3$ **(solid)** and $A=0.8L^{1.8}$, $m=0.5$, and $n=1$ **(dashed)**.

d

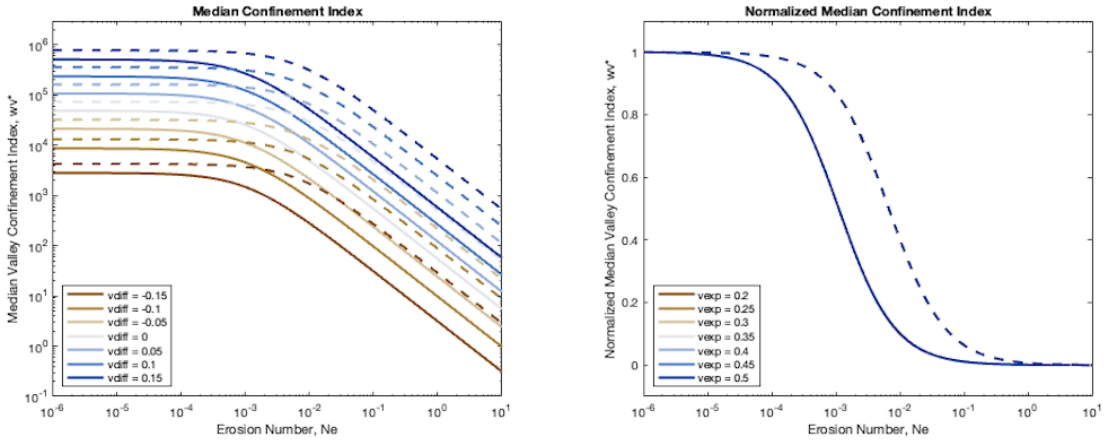

Figure S3. Modeled median wv* values and normalized median wv* values for constant valley widening coefficient, kv=2.3 (where kw=0.1), and varying valley widening exponent, c=0.2-0.5, compared to specified channel widening exponent, b=0.5. Data are consistent with Fig. 4 from the main text, but demonstrate the offset in median wv* prior to normalizing datasets for comparison to King Range data. Dashed and solid lines relate to two combinations of Hack's Law Scaling and SPIM parameterizations, $A=0.3L^2$, $m=0.5$, and $n=2/3$ **(solid)** and $A=0.8L^{1.8}$, $m=0.5$, and $n=1$ **(dashed)**.

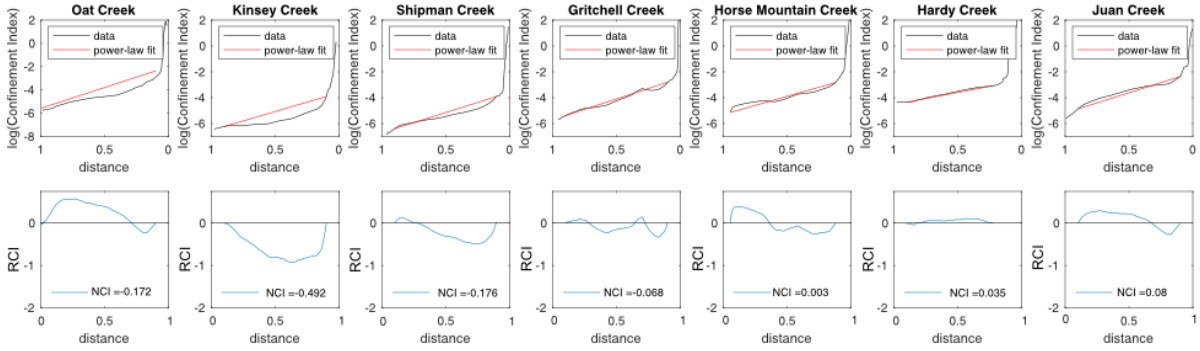

Figure S4. wv* profiles for all King Range catchments and associated residual confinement (RCI) values and NRCI values.

Data Set S1. Excel spreadsheet summarizing all data used to produce figures in the main text, full model output, and associated model-data comparison